PCCP

ROYAL SOCIETY OF CHEMISTRY

PAPER

View Article Online
View Journal | View Issue

Cite this: *Phys. Chem. Chem. Phys.*, 2025, **27**, 23400

Monoterpene flash pyrolysis reveals weakly coupled mechanistic domains and fleeting biradical intermediates

Edgar White Buenger,[a] Andras Bodi,[b] Maxi A. Burgos-Paci[c] and Paul M. Mayer *[a]

Received 15th August 2025,
Accepted 13th October 2025

DOI: 10.1039/d5cp03144c

rsc.li/pccp

The monoterpenes α-pinene, β-pinene, and limonene were in-vacuum flash pyrolyzed at 950 °C in a microreactor and the pyrolysis products were ionized and detected using vacuum ultraviolet synchrotron radiation and double imaging photoelectron photoion coincidence spectroscopy. Photoion mass-selected threshold photoelectron spectra identify the major pyrolysis products, including isoprene and cyclopentadiene (limonene and β-pinene), methylbenzenes (α-pinene), and the propargyl (β-pinene) and methyl radicals (α-pinene). Based on band intensities and photoionization cross sections, semi-quantitative product abundances were obtained. Non-negative matrix factorization shows that the pyrolysis mechanisms of α-pinene and limonene are distinct and that of β-pinene is strongly coupled to that of limonene at this temperature. This is rationalized by potential energy surface calculations that account for the main fragmentation paths. Monoterpene interconversion and limonene fragmentation to isoprene take place on the closed-shell singlet surface, while ring-opening reactions involve open-shell singlet transition states. Biradicals with quasi-degenerate triplet and singlet states, the assumed central intermediates in monoterpene decomposition, are high in energy. Although they may drive racemization and hydrogen randomization, they are not the crucial nodes previously proposed in the literature.

Introduction

Terpenes are abundant, naturally occurring hydrocarbons, built up by isoprene (C_5H_8) moieties. Monoterpenes ($C_{10}H_{16}$) consist of two isoprene units and exhibit a wide array of isomeric structures due to the three degrees of unsaturation in isoprene and the frequent formation of stereocenters during isoprene coupling, which gives rise to optical isomerism. Representative examples include the acyclic myrcene, the monocyclic limonene, and the bicyclic α-pinene, highlighting the monoterpenes' structural diversity. They are relatively volatile and readily enter the gas phase, *i.e.*, the atmosphere, when they are emitted into the environment, where they are consumed primarily through oxidation reactions with environmental oxidants, such as ozone.[1] In addition to the natural abundance and emission of terpenes, they are relevant in the food,[2] fragrance,[3] and pharmaceutical industries.[4] As fossil fuels are phased out, we turn to alternative sources of renewable energy, and monoterpenes have been considered a viable option.[5,6] The increasing intensity of forest fires worldwide due to climate change[7] as well as the prospective use case for monoterpenes as fuels means that monoterpene emissions, atmospheric oxidation,[8] and pyrolysis are expected to grow. This puts their reactivity, and particularly the pyrolysis mechanism of the most abundant monoterpenes, into research focus.

There have been numerous reports on waste tire pyrolysis, in which polyisoprene is broken down to obtain limonene,[9] to maximize limonene selectivity for economic purposes.[10] However, fundamental studies concerning limonene pyrolysis remain few and far between. Pines and Ryer investigated limonene pyrolysis at atmospheric pressure and 450 °C and observed a variety of substituted benzenes, and small amounts of isoprene and volatile gases, namely hydrogen, methane, ethane, ethylene, and propene. They proposed that biradical intermediates are first formed by homolytic bond cleavage and go on to yield the final pyrolysis products.[11] More recently, Zheng *et al.* investigated limonene pyrolysis along with that of β-pinene and myrcene and identified limonene isomerization products and minimal decomposition in the 540–600 °C temperature range, although the proportion of isoprene and non-identified products increased with temperature.[12] Bierkandt *et al.* studied limonene combustion and pyrolysis in a flow tube reactor in the 400–1000 °C range

[a] *Department of Chemistry and Biomolecular Sciences, University of Ottawa, 10 Marie Curie, Ottawa K1N 6N5, Canada. E-mail: pmmayer@uottawa.ca*
[b] *Laboratory for Synchrotron Radiation and Femtochemistry, Paul Scherrer Institute, 5232 Villigen, Switzerland*
[c] *INFIQC – CONICET, Departamento de Fisicoquímica, Universidad Nacional de Córdoba, Córdoba, Argentina*

and observed small quantities of substituted benzenes, and larger quantities of benzene and isoprene, as well as small combustion intermediates including acetylene and ethylene as pyrolysis products.[13] They also rationalized the pyrolysis mechanism by invoking the consensus biradical intermediates.

Early reports on pinene pyrolysis have shown that the α- and β-isomers yield different thermal isomerization products at intermediate temperatures, with α-pinene forming alloocimene and β-pinene providing predominantly myrcene.[14] Similar to the mechanism proposed for limonene, pinene isomers were suggested to rearrange towards the observed product through biradical intermediates.[14] Crowley and Traynor performed α-pinene pyrolysis at 420 °C and observed a variety of monoterpene isomers resulting from rearrangements, as well as the formation of methyl substituted benzene compounds.[15] Gajewski *et al.* studied the pyrolysis of deuterium-labeled α-pinene and also followed the racemization kinetics. The observation primarily relates to the relative rate of internal rotation *vs.* ring opening and closure. They concluded that a C_S biradical intermediate is the most straightforward explanation for the observations and, thus, evidence for the formation of biradical intermediates in the thermal rearrangement of α-pinene in the range of 220–260 °C.[16] Stolle, Ondrushcka and Findeisen published a study that focused on the rearrangement of α-pinene to limonene and ocimene over the range of 250–500 °C during the course of a pyrolysis experiment with GC analysis.[17] Analogous studies on β-pinene pyrolysis aimed at rationalizing the formation of myrcene, a product that is not observed in the pyrolysis of α-pinene. Kolicheski *et al.* published a study on producing myrcene through the pyrolysis of β-pinene and observed the formation of predominantly myrcene, but also limonene, and 1[7],8p-menthadiene as isomerization products, as well as smaller quantities of consecutive smaller fragmentation products over the 350–550 °C temperature range.[18] It has been suggested that the formation of myrcene from β-pinene is an endothermic but, based on its observation, necessarily entropically favourable and irreversible process at sufficiently high temperatures.[18] The proposed mechanisms for the rearrangement and the pathway for the dissociation of myrcene to butadiene and pentadiene, however, have since been questioned by other researchers in the field.[19] Coudour *et al.* identified α-pinene pyrolysis products by GC-MS at yet higher temperatures, detecting butene, isoprene, benzene, and other associated aromatic compounds at 800 °C without delving into mechanistic details.[20]

A common emphasis in monoterpene pyrolysis studies has been their rearrangement and interconversion, not so much the identification of decomposition products. The moderate temperature regimes applied in most studies are conducive to rearrangement, but not to fragmentation. However, as pyrolysis temperature rises into the range characteristic of fuel-rich wildfire conditions with residual woody fuel, the proportion of monoterpene dissociation products increases.[13]

In this work, we will carry out high-temperature pyrolysis experiments with photoelectron photoion coincidence spectroscopy detection, supplemented by theoretical calculations, to identify the dissociation products obtained through the pyrolysis of selected representative monoterpenes, namely limonene, α-pinene, and β-pinene. In the competition between low activation energy and activation entropy *vs.* high activation energy and activation entropy processes, high temperatures, characteristic of wildfires, will favor the latter. This is expected to complement previous studies carried out at lower temperatures and higher reaction times.

Methods

Pyrolysis experiments were carried out on the VUV beamline at the Swiss Light Source (SLS, Paul Scherrer Institute, Villigen, Switzerland) using the imaging photoelectron photoion coincidence endstation[21–23] and a high-temperature pyrolysis microreactor.[24] Synchrotron radiation was dispersed using a 150 grooves per mm grating; the higher harmonics of the grating being filtered out using a differentially pumped, 10 cm optical length gas filter, filled with 9 mbar of a Ne:Ar mixture. The monochromatized light, with *ca.* 5 meV energy resolution, entered the ionization chamber, where it crossed the skimmed molecular beam emanating from the microreactor. After photoionization, imaging Roent-Dek delay line detectors were employed to velocity-map photoions and photoelectrons, which were time- and position-stamped. The electron event was used as the start of the time-of-flight timer for the photoions. Photoelectrons having initially zero kinetic energy (threshold electrons) are detected at the centre of the electron imaging detector, whereas kinetic energy (“hot”) electrons are detected off-axis according to their initial lateral momentum. Hot electrons with an initial trajectory along the extraction axis also hit the centre spot. These events were subtracted from the centre mass spectra by subtracting the mass spectrum based on electrons detected in a ring around the centre spot to obtain threshold ionization mass spectra, *i.e.*, ions in coincidence with truly threshold electrons.[25] Plotting the intensity of a mass spectral peak with a particular m/z ratio from the threshold ionization mass spectrum as a function of photon energy yields the photoion mass-selected threshold photoelectron spectrum (ms-TPES).[26]

Pyrolysis experiments were performed by passing argon, at a pressure of 1 bar and a flow rate of 1 standard cubic centimeter per minute (sccm), over a vial containing the terpene at room temperature. The room temperature vapour pressure of the three terpenes is *ca.* 4–6 mbar.[27] This mixture was then diluted with 20 sccm of argon to produce a beam with approximately 0.5% terpene, which expanded through a 200 μm pinhole into the 3 cm long, 1 mm internal diameter, resistively heated SiC pyrolysis microreactor. Reactor surface temperatures have been derived based on a previously observed power dependence measured in the pyrolysis setup by a type C thermocouple (1):

$$T/^{\circ}\mathrm{C} = P/W \times 14.27 + 303 \quad (1)$$

where T is the reactor temperature and P is the heating power. The reactor temperature is considered to represent the gas temperature inside the reactor to within 100 °C.[28] The pressure and residence time in the reactor has been estimated to be 10–40 mbar and up to 100 μs, respectively.[28,29] The reactor is

placed in the source vacuum chamber, where the pressure was $\sim 5 \times 10^{-5}$ mbar during measurements. The molecular beam exiting the pyrolysis reactor passed through a 2 mm diameter skimmer into the detection chamber, kept at a pressure of 10^{-6} mbar during measurements. The reactor can be heated to temperatures between 200 and 2000 °C to explore the distribution of pyrolysis products by recording ms-TPES. The terpenes were studied at 950 °C.

Rovibrational cooling in the expansion from such microreactors has been found to be limited,[30] because of the low preexpansion pressure at the reactor nozzle.[28] The total ionization signal is therefore due in part to the barely cooled molecular beam and in part to room-temperature species that underwent collisional cooling with wall surfaces in the ionization chamber. These fractions are typically commensurate, which leads to an intermediate "effective temperature" as far as the internal energy distribution of the sample is concerned. Furthermore, previous studies with these types of reactors have concluded that the role of unimolecular *vs.* bimolecular reactions is molecule-dependent, with bimolecular reactions increasing with sample pressure for obvious reasons. Reactions involving 0.2% propionic acid in argon and 0.3% furfural in helium gave results consistent with primarily unimolecular chemistry,[31,32] while benzaldehyde pyrolysis at similar concentrations evidenced bimolecular chemistry,[31] and so did analogous acetone pyrolysis experiments.[33] Our previous work on the pyrolysis of methyl-, ethyl- and methylchloroformate did not show evidence for a meaningful amount of bimolecular reactions.[34,35]

Closed-shell singlet structures were optimized using density functional theory (DFT) with B3LYP/6-311+G(d,p) level of theory using the Gaussian 16 software suite.[36] Minimum-energy reaction paths and transition states were located using relaxed internal coordinate scans and the synchronous transit-guided quasi-Newton (STQN) method.[37] Single-point energy calculations with the CBS-QB3 composite method[38,39] were carried out for improved energetics, and are reported in the potential energy figures. There were noticeable discrepancies between, for example, the B3LYP and CBS-QB3 energies for β-pinene and myrcene. Myrcene is less stable by *ca.* 40 kJ mol^{-1} according to CBS-QB3 but only by 7 kJ mol^{-1} according to B3LYP/6-311+G(d,p). G4, M06-2X/6-311++G(d,p) and ωB97-XD/def2-TZVPP calculations confirmed the CBS-QB3 results. As B3LYP geometries feature in CBS-QB3 and G4 calculations, as well, we conclude that B3LYP geometries are acceptable, but B3LYP energetics are likely untrustworthy for these monoterpenes. Franck–Condon (FC) simulations of the ground-state ms-TPES bands of pyrolysis product candidates were also carried out using B3LYP geometries in Gaussian 16. Optimized structures shown in Fig. 2 and 3 have been uploaded to the ioChem BD database.†

Biradicals were previously proposed to play a crucial role in the conversion of monoterpenes and are characterized by two, barely coupled radical centers. The biradical energies were obtained for the triplet state using CBS-QB3. As the singlet and triplet states are quasi-degenerate, the reaction path from the singlet monoterpene to the biradical minimum may proceed on the closed-shell singlet, the open-shell singlet, or triplet surface. Therefore, we also carried out broken-symmetry open-shell singlet and triplet path calculations to determine if the open-shell potential energy surface influences unimolecular monoterpene reactivity both towards the biradicals and along the other reaction steps. Open-shell singlets (OSS) were addressed in unrestricted DFT calculations with α/β symmetry breaking by mixing β HOMO and LUMO orbitals in the initial guess, which relaxed into the closed-shell DFT result when the OSS configuration was higher in energy than the closed-shell one and yielded an open-shell solution otherwise. When symmetry-breaking led to a meaningful change in energy, OSS geometry optimizations were carried out to re-optimize the transition state geometries on the OSS surface. As B3LYP energies were found unsatisfactory and composite method calculations are not trivially applicable to these states, we evaluated the transition state energetics at the ωB97-XD/def2-TZVPP level of theory, referencing it to the related monoterpene on the potential energy surface. The broken-symmetry solution is contaminated by the triplet wave function, as seen by typical $\langle S^2 \rangle$ values of 0.7–1.0 instead of the expected 0 for a singlet. To obtain the pure singlet energy, we computed the triplet energy at the symmetry-broken optimized geometries using restricted open-shell Kohn–Sham (ROKS) ωB97-XD/def2-TZVPP calculations, and used the Yamaguchi spin decontamination correction:[40–42]

$$E_{\mathrm{OSS}} = E_{\mathrm{BS}} - \frac{\langle S^2 \rangle_{\mathrm{BS}}}{2 - \langle S^2 \rangle_{\mathrm{BS}}}(E_{\mathrm{T}} - E_{\mathrm{BS}}), \quad (2)$$

where E_{OSS} is the derived open-shell singlet energy, E_{T} is the ROKS triplet energy, E_{BS} is the broken-symmetry singlet energy and $\langle S^2 \rangle_{\mathrm{BS}}$ is the expectation value of the spin-squared operator in the broken-symmetry calculation. As discussed by David *et al.*,[43] this approach is expected to yield reliable results as long as the spin polarization of the supposedly closed-shell orbitals is minor, *i.e.*, up to $\langle S^2 \rangle \approx 1$, as was the case here. Nonetheless, the activation energies thus computed are expected to be markedly less accurate than the closed-shell and triplet biradical CBS-QB3 energies.

Results and discussion

Experimental ms-TPES and pyrolysis product identification

All recorded photoion mass-selected TPES can be found in the SI. In Fig. 1, we show the ms-TPES for *m*/*z* 68 from each of the three precursors as an example, together with a Franck–Condon simulation, in this case for isoprene.

It is evident that limonene, α- and β-pinene all produced isoprene upon pyrolysis, but the intensity of the second peak in the ms-TPES and the more gradual drop in signal intensity suggest that an additional species contributes to the *m*/*z* 68 peak in the case of α- and β-pinene. In our earlier work on isoprene pyrolysis, we observed evidence for the formation of cyclopentene, which ionizes at 9 eV and contributes the stronger band at that energy in the TPES, which may therefore be a

† https://iochem-bd.bsc.es/browse/review-collection/100/478924/ed8df8b822789fef9ca2906e.

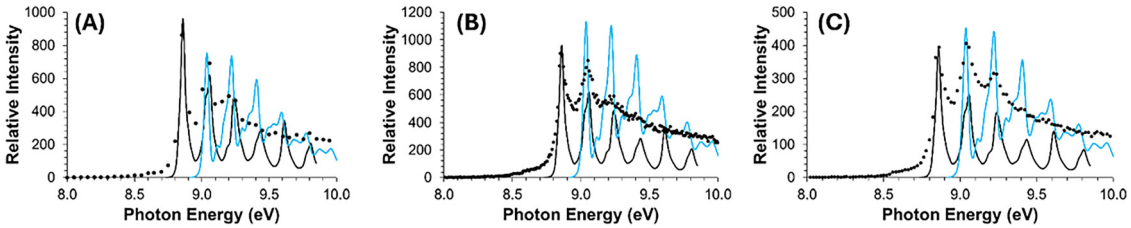

Fig. 1 Ms-TPES (markers) for *m*/*z* 68 obtained from the pyrolysis of (A) limonene, (B) α-pinene, (C) β-pinene. The FC simulations of isoprene (black line) and cyclopentadiene (blue line) have been overlaid on top of each ms-TPES. The product observed at *m*/*z* 68 has, thus, been identified as predominantly isoprene.

monoterpene pyrolysis product to account for the enhancement of the 9 eV peak.[44]

Table 1 summarizes the products observed and confirmed by FC-simulation in the pyrolysis of each terpene precursor. Aside from these peaks, up to half of the overall mass spectral signal intensity was spread over an abundance of minor peaks that could not be individually assigned. However, the major peaks can be expected to deliver a valid overall picture of the unimolecular pyrolysis chemistry of the samples to understand commonalities and differences. The fractional abundance of the confirmed products, listed in Table 1, was approximated as the intensity of the origin band in the ms-TPES, divided by the known photoionization cross sections,[45] and normalized to the sum of their total renormalized signal. Based on cursory inspection of the major products, limonene primarily dissociates into isoprene, while α- and β-pinene exhibit distinct chemistries. β-Pinene forms primarily C_5H_8 (isoprene and cyclopentene), C_4H_4 (1-buten-3-yne), and a large amount of $C_3H_3^\bullet$ (propargyl radical), while α-pinene is the "busiest" of the three terpenes, exhibiting a variety of pyrolysis products, with methyl radicals being the predominant one.

Table 1 Fractional abundances (in %) of the identified flash pyrolysis products of α-pinene, β-pinene, and limonene at 950 °C, assigned by ms-TPES. Abundances are based on cross-section corrected mass spectral signals of the ground-state TPES band (see text). The basis vectors ($\mathbf{w}_i$, renormalized to 100% in sum) from the non-negative matrix factorization, representing the mechanistic domains with their coefficients in the monoterpene pyrolysis ($\mathbf{h}_i$) giving each domain's contribution to pyrolysis. Coefficients for a two-component factorization are also given ($\mathbf{h'}_i$)

Compound	Identity	α-Pinene	β-Pinene	Limonene	$\mathbf{w}_1$	$\mathbf{w}_2$	$\mathbf{w}_3$
C_9H_{12}	Trimethylbenzene	**11.4**	0.9	1.6	0.4	11.8	1.2
C_8H_{10}	Xylene	**39.6**	2.4	7.7	3.8	**41.2**	0.7
C_7H_8	Toluene	**20.1**	2.4	6.3	4.6	**20.9**	0.2
C_6H_8	Cyclohexadiene	1.8	0.2	0.2	0.0	1.9	0.4
C_6H_6	Benzene	0.5	0.7	0.5	0.5	0.5	0.9
C_5H_8	Isoprene/ (cyclopentene)	**7.3**	**25.6**	**48.6**	**53.5**	6.7	0.0
C_5H_6	Cyclopentadiene	1.4	**15.0**	11.0	**12.2**	0.8	**17.8**
C_4H_6	1,3-Butadiene	1.3	4.6	2.3	2.4	1.1	6.7
C_4H_4	1-Buten-3-yne	0.3	2.2	2.7	3.0	0.2	1.5
C_3H_6	Propene	2.5	1.2	1.7	1.6	2.6	0.8
$C_3H_5^\bullet$	Propenyl radical	0.3	0.7	0.4	0.4	0.3	1.0
C_3H_4	Propyne	0.7	1.3	0.6	0.6	0.7	2.0
$C_3H_3^\bullet$	Propargyl radical	1.4	**30.1**	7.3	8.1	0.0	**50.9**
C_2H_4	Ethene	1.9	5.8	1.8	1.8	1.7	9.6
C_2H_2	Ethyne	0.5	2.0	1.3	1.4	0.4	2.6
$CH_3^\bullet$	Methyl radical	**9.1**	4.8	6.1	5.7	**9.3**	3.9

NMF coefficients for precursor products	$\mathbf{h'}_1$	$\mathbf{h'}_2$	$\mathbf{h}_1$	$\mathbf{h}_2$	$\mathbf{h}_3$
α-Pinene	0.00	**0.98**	0.02	**0.96**	0.02
β-Pinene	**0.82**	0.00	**0.48**	0.01	**0.52**
Limonene	**0.97**	0.18	**0.90**	0.11	0.00

Product matrix factorization

If monoterpenes were to promptly interconvert before decomposing at the high pyrolysis temperature of 950 °C, we would see the same products emanating from the reactor, independent of the precursor monoterpene. Although this is not the case, there are similarities between the experimental α-pinene, β-pinene, and limonene product vectors in Table 1. A simple measure of the similarity between the product distributions is the angle between the product vectors, computed using cosine similarity after normalizing each distribution. At 0°, the distributions are identical and at 90°, they are orthogonal to each other. The angles are 77° (α-pinene *vs.* β-pinene), 69° (α-pinene *vs.* limonene), and 40° (β-pinene *vs.* limonene). This suggests that parts of the mechanism are shared, especially between β-pinene and limonene.

Non-negative matrix factorization (NMF, as implemented in scikit-learn)[46] is motivated by the idea that complex observations can be explained as an additive, strictly non-negative combination of parts. These are obtained as basis vectors and coefficients that reconstruct the measured data, *i.e.*, the product abundances, best.[47] Because the factors cannot take negative values, each column ($\mathbf{w}_i$) naturally represents a chemically plausible mechanistic domain, and the coefficient vectors ($\mathbf{h}_i$) quantify said domain's contribution to pyrolysis. Evidence for mechanistic coupling appears when a precursor's weights are spread over more than one domain rather than concentrated in a single one. This parts-based decomposition has previously been used to interpret chemistry: positive matrix factorization work by Paatero and Tapper contributed to source apportionment in environmental chemistry,[48] and Puliyanda *et al.* recently used joint NMF to unravel coupled *versus* uncoupled reaction pathways in heavy-oil upgrading.[49]

If each sample is trivially assigned its own domain, we obtain a mathematically valid and exact but chemically uninformative decomposition with an identity matrix for the coefficients. Starting from a random or perturbed initial guess, the NMF algorithm will converge to a chemically interpretable local minimum. To avoid over-interpreting a single random initialization, we

ran NMF many times with different random seeds and chose the most representative decomposition within 1–2% of the best error, *i.e.*, one with basis profiles most similar to the other solutions. The solutions were easily reproducible and largely insensitive to initialization.

However, the first question is whether a two-component factorization reproduces the experiment well enough. The coefficients in the rank-2 factorization ($\mathbf{h}'_i$ in Table 1) suggest strong coupling between β-pinene and limonene products, and the rest of the limonene chemistry is approximated by α-pinene contributions. This, however, is a poor fit with a Euclidean reconstruction error (normalized by the Euclidean norm of the data matrix) of 27%, which shows that a third domain is necessary for a suitable reproduction of the product matrix. The three-factor basis vectors and their coefficients are also given in Table 1. Limonene and α-pinene have their own mechanistic domains ($\mathbf{w}_1$ and $\mathbf{w}_2$) in this factorization, while β-pinene chemistry is half unique ($\mathbf{w}_3$) and half coupled to limonene's domain. This provides a preliminary estimate on where the reactive flux branches out. Apparently, β-pinene will in part isomerize to limonene, but the decomposition of the other monoterpenes takes place mostly before interconversion, at least at 950 °C. If the isomerization barriers are lower in energy but associated with a lower activation entropy than the decomposition transition states, isomerization may compete more effectively at lower temperatures. Computational chemistry can be used to map the reaction paths and provide further, more tangible insights into the different mechanistic domains.

Calculated minimum energy reaction pathways

Mechanistic suggestions in the literature invoke biradicals as central early intermediates in the interconversion and decomposition of these three species. Computationally, homolytic bond breaking in a closed-shell molecule yields a biradical system, but unimolecular rearrangements may take place on the closed-shell singlet surface, as well. As the second is easier to address computationally, we first tackled the pathways on the closed-shell singlet surface. Inspired by the singlet paths, we then followed the reaction paths on the triplet surface and evaluated open-shell singlet energies for the transition states and intermediates. While we aimed to locate the lowest-lying channels using constrained bond length and angle scans as well as synchronous transit-guided quasi-Newton optimizations, per the dimensionality of the system, only a small part of the potential energy surface could be explored. However, due to the lack of a fast and robust level of theory to yield reliable energies across the potential energy surface, it is unlikely that a more aggressive PES exploration strategy using a less expensive level of theory would have yielded better results. Therefore, this balanced approach likely provides a reasonable first guess for the unimolecular thermal decomposition mechanism of monoterpenes.

The minimum energy reaction pathway for limonene fragmentation is shown in Fig. 2. The reaction towards the left is straightforward, beginning from limonene (**1**) and going over a 2.55 eV barrier (**TS1-C_5H_8**), where the cyclohexene ring is

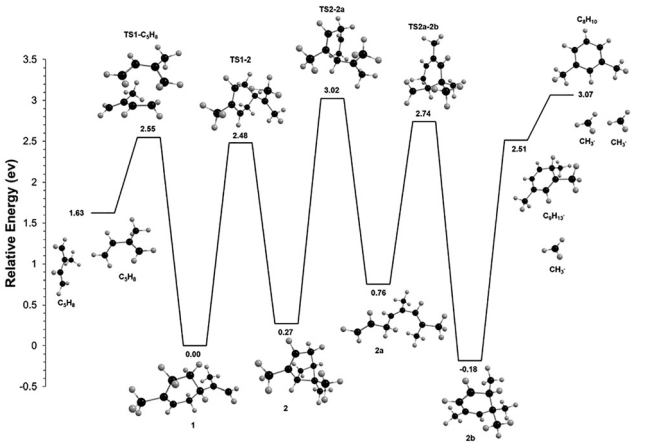

Fig. 2 Minimum energy reaction pathway calculated at the CBS-QB3//B3LYP/6-311+G(d,p) level of theory, involving limonene (**1**) and α-pinene (**2**). The pathway from **1** towards the left yields two isoprene molecules (C_5H_8). Towards the right, it connects limonene to **2**, followed by sequential losses of methyl radical to yield aromatics. Energies indicated are relative to that of **1**. A schematic representation of this mechanism can be found in Fig. S1 of the SI.

broken near the propenyl group in a retro-Diels–Alder reaction, leading to the release of two isoprene molecules (C_5H_8). This is a closed-shell fragmentation pathway with no open-shell or biradical character. Limonene can, however, also undergo isomerization by H-transfer to form a biradical. The energy of this closed-shell transition state is only 2.50 eV but the biradical is not stabilized significantly after the H atom is transferred and exhibits an energy of 1.85 eV (see potential energy surface in Fig. S3 in SI). Thus, while biradical formation is energetically allowed prior to isoprene formation in limonene, it represents a dead end in the mechanism. Limonene's facile dissociation to isoprene also explains the dominant abundance of isoprene observed experimentally in limonene pyrolysis.

Moving towards the right, limonene is connected to α-pinene by an isomerization transition state **TS1-2**, where the methyl group on the propyl moiety undergoes a 1,5-H shift and forms the C–C bridge in α-pinene. This closed-shell transition state lies at 2.33 eV, slightly lower than the 2.55 eV transition state to isoprene formation. Based on the experimental observation and the product matrix factorization, limonene barely couples to the α-pinene reactions. The limonene fragmentation (**TS1-C_5H_8**) and the **TS1-2** isomerization transition states are broadly comparable in energy, but **TS1-2** is associated with a lower activation entropy (-20 *vs.* $+25$ J K^{-1} mol^{-1} for **TS1-C_5H_8**), which allows the retro-Diels–Alder fragmentation to outcompete limonene isomerization to α-pinene at high temperatures.

Moving from structure **2**, α-pinene, towards the right, an open-chain intermediate **2a** is produced *via* elongation of one of the C–C bonds in the bicyclic bridge feature. The associated transition state, **TS(2-2a)**, is rather high in energy at 3.02 eV. Indeed, a single-point triplet–singlet gap calculation at this geometry yielded a splitting of only 0.17 eV. Only the open-shell singlet transition state, at *ca.* 2.36 eV (see SI), makes the formation of the *per se* closed-shell intermediate **2a** competitive. **2a** may then

re-cyclize by association of the terminal alkene and the central CH carbon, leading to tetramethylcyclohexadiene **2b**. Sequential bond dissociation of CH_3 groups leads to the production of the trimethylcyclohexadienyl radical and xylene, releasing two methyl radicals. This path explains the observation of the strong methyl radical signal as well as aromatic products in α-pinene pyrolysis.

Minimum energy reaction pathways calculated to account for β-pinene pyrolysis are shown in Fig. 3. Much like α-pinene, β-pinene (**3**) can also isomerize to limonene (and thus make isoprene) through **TS1-3**, which lies only at 2.22 eV. One of the CH_3 hydrogens undergoes a 1,5-H shift towards the exocyclic CH_2, resulting in **1**. The low energy of this closed-shell rearrangement transition state explains the observation of isoprene and the strong coupling between the β-pinene and limonene pyrolysis chemistry indicated by NMF, as well. Starting to the right from **3**, a rearrangement reaction is seen involving the dissociation of the bond between bicyclic bridging carbons, **TS3-3a**, at an energy of 3.02 eV. This β-pinene rearrangement is analogous to the one calculated in α-pinene, but it leads to **3a**, myrcene, due to the position of the double bond. We did not detect myrcene in β-pinene pyrolysis, and do not have data on myrcene pyrolysis under comparable conditions, but propargyl radicals, an abundant product in the β-pinene reaction domain, represent a likely sequential fragmentation product of myrcene. Because of the linear chain and the comparable bond energies in myrcene, its pyrolysis mechanism is expected to be convoluted, and we did not endeavor to unveil it solely computationally. While this path over a closed-shell transition state leads to a major pyrolysis product of β-pinene known in the literature, its activation energy is prohibitively high.

Although the triplet single-point energy at **TS3-3a** was found to be 0.25 eV higher, an open-shell rearrangement transition state was found at 2.56 eV (SI). In fact, we also located a lower-lying open-shell path, with a much lower barrier of *ca.* 1.90 eV, leading to ψ-limonene. This activation energy is slightly lower than the 2.22 eV isomerization activation energy to limonene. β-Pinene can be thermally converted to 80% myrcene at 450 °C with 11% limonene as co-product, and ψ-limonene is not a major pyrolysis product.[50] Therefore, the overall activation energy to myrcene formation cannot be significantly higher than *ca.* 2 eV, the closed-shell transition state **TS3-3a** to limonene formation, which is followed dominantly by isoprene release. In fact, the economically feasible conversion of β-pinene to myrcene at lower temperatures, combined with the NMF result of *ca.* 50 : 50 β-pinene and limonene mechanistic contributions to the β-pinene flash pyrolysis products tells us that isomerization to myrcene is dominant at low energies and outcompeted by the looser but higher-energy isomerization process to limonene at our elevated temperatures and short reaction times. Therefore, the transition state to myrcene formation should be tighter and at a lower energy than the isomerization transition state to limonene. Consequently, either the true transition state to myrcene is lower than the OSS transition state we located at 2.56 eV, or ψ-limonene is an intermediate on the way to myrcene formation. In the absence of pyrolysis data on ψ-limonene, we have not explored its thermal decomposition pathways further. These insights and the open-shell transition states driving some of the discussed decomposition paths call for a discussion of the "biradical" intermediates as invoked ubiquitously in the mechanistic discussions of terpene pyrolysis in the literature.

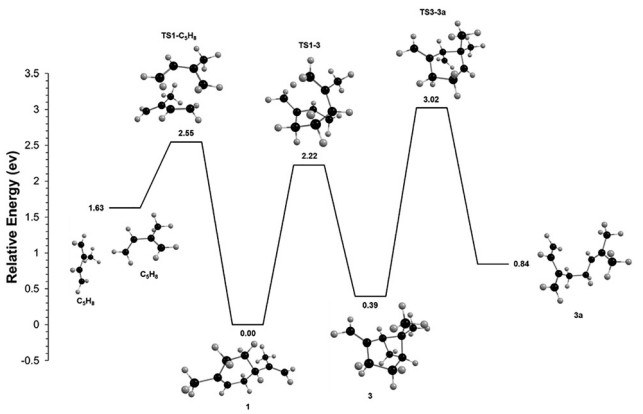

Fig. 3 Minimum energy reaction pathway calculated at the CBS-QB3//B3LYP/6-311+G(d,p) level of theory, involving limonene (**1**) and β-pinene (**3**). Isoprene formation from **1** is the same as in Fig. 2. The transition state towards the right connects limonene and β-pinene, which can also rearrange to myrcene (**3a**). Energy values are relative to that of limonene. A schematic representation of this mechanism can be found in Fig. S2 of the SI.

On the role of biradicals

Apart from the open-shell singlet ring-opening transition states discussed above, triplet and OSS minima and transition states along the potential energy surfaces in Fig. 2 and 3 were found to be, in part significantly, higher in energy than the closed-shell singlets. The central biradical intermediates proposed by, *e.g.*, Gajewski *et al.*[16] are distinct from the structures along our PES and correspond to ring-opening of the bicyclic α- and β-pinene to a configuration with two hypovalent carbons with remote radical centers and quasi-degenerate open-shell singlet and triplet electronic configurations. We have also considered the biradical isomer of limonene by H-transfer and found that the biradicals' energy was in the 1.85–1.90 eV range relative to limonene. The corresponding isomerization transition states were found to be on the closed-shell surface at 2.33 eV for α-pinene and at 2.50 eV for limonene. While the former corresponds to a bond breaking, biradical formation in limonene requires a H-transfer, therefore a tight transition state. For β-pinene, an OSS transition state was found at a remarkably low energy of 1.90 eV, suggesting that biradical formation is kinetically allowed at its energetic threshold of 2.26 eV. Thus, biradical formation is generally energetically allowed in the energy range of the other isomerization/fragmentation processes, although it takes place over a tight transition state in limonene. Based on the harmonic free energies and activation free energies, evaluated using thermo.py by Irikura,[51] we calculated equilibrium constants and rate constants as a function of temperature to gain further insights into the biradicals' role. As shown in Fig. S4, the equilibrium fractional abundance of the biradical derived from β-pinene is on the order of 10^{-10} at

temperatures where thermal dissociation does not yet convert the precursor into lighter fragments quantitatively. Statistical rates for ring opening in α-pinene and isoprene formation in limonene are also at least an order of magnitude higher than for biradical formation. The biradical energies are expected to be accurately reported by CBS-QB3. Consequently, biradicals are unlikely to be present in detectable amounts, irrespective of the experimental conditions. Furthermore, because of their high energies, they are not fragmentation or isomerization intermediates. However, because of the errors in the harmonic approximation and the uncertainties in the activation energies, we cannot exclude that biradical formation rates are higher and that they may still play a role in racemization in both pinenes.

Thus, the interconversion of the α-pinene/limonene/β-pinene system as well as the straightforward fragmentation of the limonene to isoprene takes place on the closed-shell singlet surface. Although the assumed biradical mechanisms are suitable to fit the reaction kinetics[12,17,19] and account for the racemization of the sample as well as deuterium scrambling,[16] our results suggest that biradicals may be responsible for racemization and hydrogen scrambling (as statistical rates may be off by more than an order of magnitude), but do not play a role in driving thermal decomposition chemistry (because of the high biradical energies). Furthermore, even if equilibrium biradical concentrations are reached, they will remain undetectable trace components in the reactive mixture at all temperatures. This insight underlines the importance of computational confirmation of the viability of assumed reaction intermediates.

At the same time, as mentioned earlier, the ring-opening transition states of α- as well as β-pinene are open-shell singlets, which brings the calculated surface more in line with the experimental observations. Open-shell singlet transition states appear to play a major role in driving monoterpene unimolecular thermal decomposition, but not their isomerization. These transition states, however, are not biradicals and exhibit substantial singlet–triplet gaps.

Conclusion

The major flash pyrolysis products of limonene, α- and β-pinene were identified at a pyrolysis temperature of 950 °C based on their ms-TPES, recorded by imaging photoelectron photoion spectroscopy. A semi-quantitative analysis yielded a product matrix, which showed isoprene as the predominant product in limonene pyrolysis, strong aromatics as well as methyl radical signals in α-pinene thermal decomposition, and propargyl radicals and cyclopentadiene as well as isoprene as the most important β-pinene fragmentation products. Non-negative matrix factorization with two basis vectors could not reproduce the product matrix faithfully, confirming that the three samples fragment according to three mechanistic domains. NMF also indicated that these may be thought of as the limonene mechanism (retro-Diels–Alder reaction to isoprene), the α-pinene mechanism to aromatics, and about half of the β-pinene reactive flux proceeds *via* the limonene mechanism while the other half ultimately yields propargyl and cyclopentadiene as major products, likely over a myrcene intermediate. While NMF analysis yielded proof-of-principle mechanistic insights that were in line with the computational results, it was inherently limited by the low dimension of the data sets. Temperature-dependent product matrices of more monoterpene isomers would have yielded better-defined insights, but experimental developments, such as quantification approaches based on measurements at only one or a few photon energies, would be needed for more expansive data sets to be within reach.

We have explored the closed-shell singlet potential energy surface to identify the main monoterpene interconversion and fragmentation mechanisms using density functional theory and the CBS-QB3 method for single-point energies. This exploration was guided by the observed pyrolysis products, and only a small part of the phase space could be covered. Alternative, automatic reaction kinetics approaches[52] could account for a larger part of the mechanism, including the minor products, if coupled with a methods strategy that addresses closed- and open-shell singlet as well as triplet states consistently. Still, the isomerization reactions and the major limonene pathway, the formation of isoprene, are well-described by this approach. From α- and β-pinene, open-shell singlet ring-opening transition states lead to fragmentation at comparable energies, explaining the competition between interconversion and fragmentation, the latter of which dominates in α-pinene, and a combination is seen in β-pinene. Biradicals are very high in energy to be intermediates in thermal decomposition. While their formation is energetically allowed at 1.80–1.95 eV above limonene over moderate or even submerged transition states, statistical equilibrium constant and rate constant calculations suggest that they are at most fleeting species in the reactive mixture and not major fragmentation intermediates they were made out to be. Thus, we show that the flash pyrolysis of monoterpenes is driven by isomerization and fragmentation transition states, of which ring-opening transition states often have open-shell character and, contrary to the longstanding paradigm, biradical intermediates, while they may account for racemization, are unlikely to play a major role in thermal decomposition.

Conflicts of interest

There are no conflicts to declare.

Data availability

Supplementary information (SI): all experimentally-derived mass-selected threshold photoelectron spectra, together with Franck–Condon simulations. Schematic reaction mechanisms (Fig. S1 and S2), the potential energy surface with open-shell singlet transition states and biradical energetics (Fig. S3) and Fig. S4: equilibrium constant as a function of temperature for biradical formation from β-pinene and RRKM rate constants for ring opening in α-pinene, isoprene formation from limonene and biradical formation. See DOI: **https://doi.org/10.1039/d5cp03144c**.

Data is available from the archives of the Swiss Light Source. Contact Andras Bodi at the Paul Scherrer Institut.

Acknowledgements

MABP thanks Secyt-UNC and CONICET for the financial support. PMM thanks the Natural Sciences and Engineering Research Council of Canada for continuing financial support, the Digital Research Alliance of Canada for computational resources, and the team at the VUV beamline of the Swiss Light Source for their experimental support, especially during the COVID-19 pandemic, and their enabling of remote experimentation.

References

1 J. Yu, R. J. Griffin, D. R. Cocker, R. C. Flagan, J. H. Seinfeld and P. Blanchard, Observation of Gaseous and Particulate Products of Monoterpene Oxidation in Forest Atmospheres, *Geophys. Res. Lett.*, 1999, **26**(8), 1145–1148, DOI: 10.1029/1999GL900169.

2 J. F. R. De Alvarenga, B. Genaro, B. L. Costa, E. Purgatto, C. Manach and J. Fiamoncini, Monoterpenes: Current Knowledge on Food Source, Metabolism, and Health Effects, *Crit. Rev. Food Sci. Nutr.*, 2023, **63**(10), 1352–1389, DOI: 10.1080/10408398.2021.1963945.

3 C. G. Vieira, E. N. Dos Santos and E. V. Gusevskaya, Synthesis of Fragrance Compounds from Acyclic Monoterpenes: Rhodium Catalyzed Hydroformylation and Tandem Hydroformylation/Acetalization of Linalool and β-Citronellene, *Appl. Catal., A*, 2013, **466**, 208–215, DOI: 10.1016/j.apcata.2013.06.037.

4 A. Koziol, A. Stryjewska, T. Librowski, K. Salat, M. Gawel, A. Moniczewski and S. Lochynski, An Overview of the Pharmacological Properties and Potential Applications of Natural Monoterpenes, *Mini-Rev. Med. Chem.*, 2015, **14**(14), 1156–1168, DOI: 10.2174/1389557514666141127145820.

5 B. G. Harvey, M. E. Wright and R. L. Quintana, High-Density Renewable Fuels Based on the Selective Dimerization of Pinenes, *Energy Fuels*, 2010, **24**(1), 267–273, DOI: 10.1021/ef900799c.

6 M. Kumar, C. Tung Chong and S. Karmakar, Comparative Assessment of Combustion Characteristics of Limonene, Jet A-1 and Blends in a Swirl-Stabilized Combustor under the Influence of Pre-Heated Swirling Air, *Fuel*, 2022, **316**, 123350, DOI: 10.1016/j.fuel.2022.123350.

7 M. Turco, J. T. Abatzoglou, S. Herrera, Y. Zhuang, S. Jerez, D. D. Lucas, A. AghaKouchak and I. Cvijanovic, Anthropogenic Climate Change Impacts Exacerbate Summer Forest Fires in California, *Proc. Natl. Acad. Sci. U. S. A.*, 2023, **120**(25), e2213815120, DOI: 10.1073/pnas.2213815120.

8 L. Courty, K. Chetehouna, L. Lemée, C. Mounaïm-Rousselle, F. Halter and J. P. Garo, Pinus Pinea Emissions and Combustion Characteristics of Limonene Potentially Involved in Accelerating Forest Fires, *Int. J. Therm. Sci.*, 2012, **57**, 92–97, DOI: 10.1016/j.ijthermalsci.2012.02.012.

9 B. Danon, P. Van Der Gryp, C. E. Schwarz and J. F. Görgens, A Review of Dipentene (Dl-Limonene) Production from Waste Tire Pyrolysis, *J. Anal. Appl. Pyrolysis*, 2015, **112**, 1–13, DOI: 10.1016/j.jaap.2014.12.025.

10 S. Farzad, M. Mandegari and J. F. Görgens, A Novel Approach for Valorization of Waste Tires into Chemical and Fuel (Limonene and Diesel) through Pyrolysis: Process Development and Techno Economic Analysis, *Fuel Process. Technol.*, 2021, **224**, 107006, DOI: 10.1016/j.fuproc.2021.107006.

11 H. Pines and J. Ryer, Studies in the Terpene Series. XXIII. Pyrolysis of (d-Limonene and of Related Hydrocarbons. Mechanisms of Pyrolysis, *J. Am. Chem. Soc.*, 1955, **77**, 4370–4375, DOI: 10.1021/ja01621a055.

12 H. Zheng, J. Chen, C. Li, J. Chen, Y. Wang, S. Zhao and Y. Zeng, Mechanism and Kinetics of the Pyrolysis of β-Pinene to Myrcene, *J. Anal. Appl. Pyrolysis*, 2017, **123**, 99–106, DOI: 10.1016/j.jaap.2016.12.020.

13 T. Bierkandt, N. Gaiser, J. Bachmann, P. Oßwald and M. Köhler, Terpene Speciation: Analytical Insights into the Oxidation and Pyrolysis of Limonene and 1,8-Cineole via Molecular-Beam Mass Spectrometry, *Combust. Flame*, 2025, **272**, 113854, DOI: 10.1016/j.combustflame.2024.113854.

14 R. L. Burwell, The Mechanism of the Pyrolyses of Pinenes, *J. Am. Chem. Soc.*, 1951, **73**(9), 4461–4462, DOI: 10.1021/ja01153a508.

15 K. J. Crowley and S. G. Traynor, Ground State Sigmatropic and Electrocyclic Rearrangements in Some Monoterpenes, *Tetrahedron*, 1978, **34**(18), 2783–2789, DOI: 10.1016/0040-4020(78)88420-8.

16 J. J. Gajewski, I. Kuchuk, C. Hawkins and R. Stine, The Kinetics, Stereochemistry, and Deuterium Isotope Effects in the a-Pinene Pyrolysis. Evidence for Incursion of Multiple Conformations of a Diradical, *Tetrahedron*, 2002, **58**, 6943–6950, DOI: 10.1016/S0040-4020(02)00676-2.

17 A. Stolle, B. Ondruschka and M. Findeisen, Mechanistic and Kinetic Insights into the Thermally Induced Rearrangement of α-Pinene, *J. Org. Chem.*, 2008, **73**(21), 8228–8235, DOI: 10.1021/jo8012995.

18 M. B. Kolicheski, L. C. Cocco, D. A. Mitchell and M. Kaminski, Synthesis of Myrcene by Pyrolysis of β-Pinene: Analysis of Decomposition Reactions, *J. Anal. Appl. Pyrolysis*, 2007, **80**(1), 92–100, DOI: 10.1016/j.jaap.2007.01.005.

19 A. Stolle and B. Ondruschka, Comment to the Paper "Synthesis of Myrcene by Pyrolysis of b-Pinene: Analysis of Decomposition Reactions" by M. B. Kolicheski *et al.* [J. Anal. Appl. Pyrol. 80 (2007) 92–100], *J. Anal. Appl. Pyrolysis*, 2008, 136–138.

20 B. Coudour, K. Chetehouna, L. Lemée, P. Bertin and J.-P. Garo, Thermal Degradation of α-Pinene Using a Py–GC/MS, *J. Therm. Anal. Calorim.*, 2019, **137**(4), 1315–1328, DOI: 10.1007/s10973-019-08028-8.

21 A. Bodi, P. Hemberger, T. Gerber and B. Sztáray, A New Double Imaging Velocity Focusing Coincidence Experiment: *I* 2PEPICO, *Rev. Sci. Instrum.*, 2012, **83**(8), 083105, DOI: 10.1063/1.4742769.

22 B. Sztáray, K. Voronova, K. G. Torma, K. J. Covert, A. Bodi, P. Hemberger, T. Gerber and D. L. Osborn, CRF-PEPICO: Double Velocity Map Imaging Photoelectron Photoion Coincidence Spectroscopy for Reaction Kinetics Studies, *J. Chem. Phys.*, 2017, **147**(1), 013944, DOI: 10.1063/1.4984304.

23 A. Bodi, P. Hemberger and J. Pérez-Ramírez, Photoionization Reveals Catalytic Mechanisms, *Nat. Catal.*, 2022, **5**(10), 850–851, DOI: **10.1038/s41929-022-00847-7**.

24 P. Hemberger, V. B. F. Custodis, A. Bodi, T. Gerber and J. A. Van Bokhoven, Understanding the Mechanism of Catalytic Fast Pyrolysis by Unveiling Reactive Intermediates in Heterogeneous Catalysis, *Nat. Commun.*, 2017, **8**(1), 15946, DOI: **10.1038/ncomms15946**.

25 B. Sztáray and T. Baer, Suppression of Hot Electrons in Threshold Photoelectron Photoion Coincidence Spectroscopy Using Velocity Focusing Optics, *Rev. Sci. Instrum.*, 2003, **74**(8), 3763–3768, DOI: **10.1063/1.1593788**.

26 P. Hemberger, A. Bodi, T. Bierkandt, M. Köhler, D. Kaczmarek and T. Kasper, Photoelectron Photoion Coincidence Spectroscopy Provides Mechanistic Insights in Fuel Synthesis and Conversion, *Energy Fuels*, 2021, **35**(20), 16265–16302, DOI: **10.1021/acs.energyfuels.1c01712**.

27 W. E. Acree and J. S. Chickos, Phase Transition Enthalpy Measurements of Organic and Organometallic Compounds. in *NIST Chemistry WebBook, NIST Standard Reference Database Number 69*, ed. P. J. Linstrom and W. G. Mallard, National Institute of Standards and Technology, Gaithersburg, MD, 20899 (retrieved October 15, 2025).

28 Q. Guan, K. N. Urness, T. K. Ormond, D. E. David, G. Barney Ellison and J. W. Daily, The Properties of a Micro-Reactor for the Study of the Unimolecular Decomposition of Large Molecules, *Int. Rev. Phys. Chem.*, 2014, **33**(4), 447–487, DOI: **10.1080/0144235X.2014.967951**.

29 S. Grimm, S.-J. Baik, P. Hemberger, A. Bodi, A. M. Kempf, T. Kasper and B. Atakan, Gas-Phase Aluminium Acetylacetonate Decomposition: Revision of the Current Mechanism by VUV Synchrotron Radiation, *Phys. Chem. Chem. Phys.*, 2021, **23**(28), 15059–15075, DOI: **10.1039/D1CP00720C**.

30 P. Hemberger, X. Wu, Z. Pan and A. Bodi, Continuous Pyrolysis Microreactors: Hot Sources with Little Cooling? New Insights Utilizing Cation Velocity Map Imaging and Threshold Photoelectron Spectroscopy, *J. Phys. Chem. A*, 2022, **126**(14), 2196–2210, DOI: **10.1021/acs.jpca.2c00766**.

31 A. K. Vasiliou, J. H. Kim, T. K. Ormond, K. M. Piech, K. N. Urness, A. M. Scheer, D. J. Robichaud, C. Mukarakate, M. R. Nimlos, J. W. Daily, Q. Guan, H.-H. Carstensen and G. B. Ellison, Biomass Pyrolysis: Thermal Decomposition Mechanisms of Furfural and Benzaldehyde, *J. Chem. Phys.*, 2013, **139**(10), 104310, DOI: **10.1063/1.4819788**.

32 C. O. Rogers, K. S. Lockwood, Q. L. D. Nguyen and N. J. Labbe, Diol Isomer Revealed as a Source of Methyl Ketene from Propionic Acid Unimolecular Decomposition, *Int. J. Chem. Kinet.*, 2021, **53**(12), 1272–1284, DOI: **10.1002/kin.21532**.

33 D. P. Zaleski, R. Sivaramakrishnan, H. R. Weller, N. A. Seifert, D. H. Bross, B. Ruscic, K. B. Moore, S. N. Elliott, A. V. Copan, L. B. Harding, S. J. Klippenstein, R. W. Field and K. Prozument, Substitution Reactions in the Pyrolysis of Acetone Revealed through a Modeling, Experiment, Theory Paradigm, *J. Am. Chem. Soc.*, 2021, **143**(8), 3124–3142, DOI: **10.1021/jacs.0c11677**.

34 B. Lowe, A. L. Cardona, J. Salas, A. Bodi, M. A. Burgos Paci and P. M. Mayer, Probing the Pyrolysis of Methyl Formate in the Dilute Gas Phase by Synchrotron Radiation and Theory, *J. Mass Spectrom.*, 2022, **57**(6), e4868, DOI: **10.1002/jms.4868**.

35 B. Lowe, A. L. Cardona, A. Bodi, P. M. Mayer and M. A. Burgos Paci, The Unimolecular Chemistry of Methyl Chloroformate Ions and Neutrals: A Story of Near-Threshold Decomposition, *J. Am. Soc. Mass Spectrom.*, 2023, **34**(12), 2831–2839, DOI: **10.1021/jasms.3c00334**.

36 M. J. Frisch, G. W. Trucks, H. B. Schlegel, G. E. Scuseria, M. A. Robb, J. R. Cheeseman, G. Scalmani, V. Barone, G. A. Petersson, H. Nakatsuji, X. Li, M. Caricato, A. V. Marenich, J. Bloino, B. G. Janesko, R. Gomperts, B. Mennucci, H. P. Hratchian, J. V. Ortiz, A. F. Izmaylov, J. L. Sonnenberg, D. Williams-Young, F. Ding, F. Lipparini, F. Egidi, J. Goings, B. Peng, A. Petrone, T. Henderson, D. Ranasinghe, V. G. Zakrzewski, J. Gao, N. Rega, G. Zheng, W. Liang, M. Hada, M. Ehara, K. Toyota, R. Fukuda, J. Hasegawa, M. Ishida, T. Nakajima, Y. Honda, O. Kitao, H. Nakai, T. Vreven, K. Throssell, J. A. Montgomery Jr., J. E. Peralta, F. Ogliaro, M. J. Bearpark, J. J. Heyd, E. N. Brothers, K. N. Kudin, V. N. Staroverov, T. A. Keith, R. Kobayashi, J. Normand, K. Raghavachari, A. P. Rendell, J. C. Burant, S. S. Iyengar, J. Tomasi, M. Cossi, J. M. Millam, M. Klene, C. Adamo, R. Cammi, J. W. Ochterski, R. L. Martin, K. Morokuma, O. Farkas, J. B. Foresman and D. J. Fox, *Gaussian 16 Rev. C.01*, 2016.

37 C. Peng and H. Bernhard Schlegel, Combining Synchronous Transit and Quasi-Newton Methods to Find Transition States, *Isr. J. Chem.*, 1993, **33**(4), 449–454, DOI: **10.1002/ijch.199300051**.

38 J. W. Ochterski, G. A. Petersson and J. A. Montgomery, A Complete Basis Set Model Chemistry. V. Extensions to Six or More Heavy Atoms, *J. Chem. Phys.*, 1996, **104**(7), 2598–2619, DOI: **10.1063/1.470985**.

39 J. A. Montgomery, M. J. Frisch, J. W. Ochterski and G. A. Petersson, A Complete Basis Set Model Chemistry. VI. Use of Density Functional Geometries and Frequencies, *J. Chem. Phys.*, 1999, **110**(6), 2822–2827, DOI: **10.1063/1.477924**.

40 K. Yamaguchi, H. Fukui and T. Fueno, Molecular orbital (MO) theory for magnetically interacting organic compounds. Ab-initio MO calculations of the effective exchange integrals for cyclophane-type carbene dimers, *Chem. Lett.*, 1986, (4), 625–628, DOI: **10.1246/cl.1986.625**.

41 K. Yamaguchi, Y. Takahara, T. Fueno and K. N. Houk, Extended Hartree-Fock (EHF) Theory of Chemical Reactions: III. Projected Møller-Plesset (PMP) Perturbation Wavefunctions for Transition Structures of Organic Reactions, *Theor. Chim. Acta*, 1988, **73**(5–6), 337–364, DOI: **10.1007/BF00527740**.

42 S. Yamanaka, M. Okumura, M. Nakano and K. Yamaguchi, EHF Theory of Chemical Reactions Part 4. UNO CASSCF, UNO CASPT2 and R(U)HF Coupled-Cluster (CC) Wavefunctions, *J. Mol. Struct.*, 1994, **310**, 205–218.

43 G. David, G. Trinquier and J.-P. Malrieu, Consistent Spin Decontamination of Broken-Symmetry Calculations of Diradicals, *J. Chem. Phys.*, 2020, **153**(19), 194107, DOI: **10.1063/5.0029201**.

44 E. W. Buenger, A. Bodi, M. A. Burgos-Paci and P. M. Mayer, Cyclopentene and Cyclopentadiene Formation in Isoprene Pyrolysis, *Phys. Chem. Chem. Phys.*, 2024, **26**(36), 23971–23978, DOI: **10.1039/D4CP02798A**.

45 Y. Li; J. Yang and Z. Cheng, ed. JiuZhong Yang and Combustion Team. Photonionization Cross Section Database (Version 2.0), 2017. **https://flame.nsrl.ustc.edu.cn/database/**.

46 F. Pedregosa, G. Varoquaux, A. Gramfort, V. Michel, B. Thirion, O. Grisel, M. Blondel, P. Prettenhofer, R. Weiss, V. Dubourg, J. Vanderplas, A. Passos and D. Cournapeau, Scikit-Learn: Machine Learning in Python, *J. Mach. Learn. Res.*, 2011, **12**, 2825–2830.

47 D. D. Lee and H. S. Seung, Learning the Parts of Objects by Non-Negative Matrix Factorization, *Nature*, 1999, **401**(6755), 788–791, DOI: **10.1038/44565**.

48 P. Paatero and U. Tapper, Positive Matrix Factorization: A Non-negative Factor Model with Optimal Utilization of Error Estimates of Data Values, *Environmetrics*, 1994, **5**(2), 111–126, DOI: **10.1002/env.3170050203**.

49 A. Puliyanda, K. Sivaramakrishnan, Z. Li, A. De Klerk and V. Prasad, Data Fusion by Joint Non-Negative Matrix Factorization for Hypothesizing Pseudo-Chemistry Using Bayesian Networks, *React. Chem. Eng.*, 2020, **5**(9), 1719–1737, DOI: **10.1039/d0re00147c**.

50 D. Yin, D. Yin, Z. Fu and Q. Li, The Regioselectivity of Diels–Alder Reaction of Myrcene with Carbonyl-Containing Dienophiles Catalysed by Lewis Acids, *J. Mol. Catal. A: Chem.*, 1999, **148**(1–2), 87–95, DOI: **10.1016/s1381-1169(99)00113-2**.

51 K. K. Irikura THERMO.PY. Natl. Inst. Stand. Technol 2020.

52 J. Zádor, C. Martí, R. Van De Vijver, S. L. Johansen, Y. Yang, H. A. Michelsen and H. N. Najm, Automated Reaction Kinetics of Gas-Phase Organic Species over Multiwell Potential Energy Surfaces, *J. Phys. Chem. A*, 2023, **127**(3), 565–588, DOI: **10.1021/acs.jpca.2c06558**.